ARL-TR-10075 • MAR 2025

A Quasi-1D Three-Phase Deflagration Model with Detailed Finite-Rate Chemical Kinetics Mechanisms: Frozen Ozone (Revisited) and Plateau Burning Rates

by Michael J. McQuaid

NOTICES

Disclaimers

The findings in this report are not to be construed as an official Department of the Army position unless so designated by other authorized documents.

Citation of manufacturer's or trade names does not constitute an official endorsement or approval of the use thereof.

Destroy this report when it is no longer needed. Do not return it to the originator.

ARL-TR-10075 ● MAR 2025

A Quasi-1D Three-Phase Deflagration Model with Detailed Finite-Rate Chemical Kinetics Mechanisms: Frozen Ozone (Revisited) and Plateau Burning Rates

Michael J. McQuaid
DEVCOM Army Research Laboratory

REPORT DOCUMENTATION PAGE

1. REPORT DATE	2. REPORT TYPE	3. DATES COVERED	
		START DATE	END DATE
March 2025	Technical Report	August 2024	February 2025

4. TITLE AND SUBTITLE
A Quasi-1D Three-Phase Deflagration Model with Detailed Finite-Rate Chemical Kinetics Mechanisms: Frozen Ozone (Revisited) and Plateau Burning Rates

5a. CONTRACT NUMBER	5b. GRANT NUMBER	5c. PROGRAM ELEMENT NUMBER
5d. PROJECT NUMBER	**5e. TASK NUMBER**	**5f. WORK UNIT NUMBER**

6. AUTHOR(S)
Michael J. McQuaid

7. PERFORMING ORGANIZATION NAME(S) AND ADDRESS(ES)
DEVCOM Army Research Laboratory
ATTN: FCDD-RLA-WC
Aberdeen Proving Ground, MD 21005

8. PERFORMING ORGANIZATION REPORT NUMBER
ARL-TR-10075

9. SPONSORING/MONITORING AGENCY NAME(S) AND ADDRESS(ES)	10. SPONSOR/MONITOR'S ACRONYM(S)	11. SPONSOR/MONITOR'S REPORT NUMBER(S)

12. DISTRIBUTION/AVAILABILITY STATEMENT
DISTRIBUTION STATEMENT A. Approved for public release: distribution unlimited.

13. SUPPLEMENTARY NOTES

14. ABSTRACT
As a step toward establishing a physics-based modeling framework with the potential to reliably predict the pressure-dependent burning rates $[r(P)]$ of catalyzed double-base propellants (DBPs), a quasi-1D three-phase model for simulating the deflagration of frozen (solid) ozone ($O_{3,s}$) was formulated and applied. To identify changes a catalyst would have to produce in the thermochemical kinetics of the system's liquid phase (LP) to yield both "super-rate" and "plateau" burning-rate regions, the impacts of heuristic changes to the LP's kinetics mechanism were calculated and assessed. A mechanism that produced an $r(P)$ plot with both super-rate and plateau regions was predicated on limiting chemical reactivity to a reversible one-step reaction for the decomposition of liquid ozone ($O_{3,l}$) to O_l and $O_{2,l}$ and lowering the enthalpy of O_l from a best guess. In addition, the capacity of those predicates to produce a super-rate and plateau could be further enhanced by decreasing the liquid-to-gas volatilization rate in proportion to $O_{3,l}$'s decomposition. The correspondence between this variation of the model and a chelation/complex-formation theory proposed to explain the super-rate burning of catalyzed-DBPs is apparent. Moreover, the model provides additional support for this theory by demonstrating that it can concomitantly produce a plateau region.

15. SUBJECT TERMS
Weapons Sciences, rocket propulsion, deflagration modeling, combustion, chemical kinetics

16. SECURITY CLASSIFICATION OF:			17. LIMITATION OF ABSTRACT	18. NUMBER OF PAGES
a. REPORT	b. ABSTRACT	C. THIS PAGE		
UNCLASSIFIED	UNCLASSIFIED	UNCLASSIFIED	UU	41

19a. NAME OF RESPONSIBLE PERSON
Michael J. McQuaid

19b. PHONE NUMBER *(Include area code)*
(410) 278-6185

STANDARD FORM 298 (REV. 5/2020)
Prescribed by ANSI Std. Z39.18

Contents

List of Figures

List of Tables

Acknowledgments

As with all my deflagration modeling work, I am grateful to Dr. Martin Miller (DEVCOM Army Research Laboratory, retired) for leading the way. Had he not developed and applied a three-phase model, I doubt it would have ever occurred to me that such an effort might be worthwhile. I am also grateful to Dr. Christopher Stone (ARL), who pointed out an error in my initial formulation of one of the model's boundary conditions and provided other feedback that improved this report.

1. Introduction

In the course of writing a user's manual for the CYCLOPS3_WPSB program for predicting the burning (or regression) rates (r) of energetic materials (McQuaid and Stone 2024), I exchanged emails with the originator of the CYCLOPS framework—Dr. Martin Miller (U.S. Army Combat Capabilities Development Command Army Research Laboratory, retired)—including in mine some highlights of the framework's evolution and application subsequent to his retirement. In one of his emails, he mentioned that CYCLOPS's two-phase framework was the contraction of a three-phase combustion model he had formulated and employed to predict frozen (solid) ozone's ($O_{3,s}$'s) burning rate as a function of pressure (P) (Miller 1995, 1997). He also noted that he had intended to use that model to calculate burning rates for RDX. However, believing management was impatient to see more practical applications, he started to think about how to predict the burning rates of gun propellants. The CYCLOPS framework ensued (Miller and Anderson 2000, 2004).

For my part, I first learned about Hertz–Langmuir–Knudsen (HLK) relationships for calculating liquid-to-gas volatilization rates from Dr. Miller's summary of his three-phase model (Miller 1997) and efforts to develop and integrate such relationships into various physics-based combustion models were rewarded (McQuaid and Chen 2016a, 2016b; McQuaid et al. 2017). However, until his email, I had not given serious thought to formulating and applying a three-phase model. The CYCLOPS framework had well-served my research needs, and it was difficult for me to imagine that the effort required to include a third phase would pay dividends. Indeed, I was involved in one study in which the CYCLOPS framework was employed to simulate the deflagration of RDX, and good agreement between measured and predicted $r(P)$ values was obtained (Veals et al. 2019). Moreover, in studies where good agreement between measured and predicted values was not observed, better-founded representations of the dynamics at the interface between the condensed and gas phases appeared capable of explaining most discrepancies (McQuaid and Chen 2014).

Those observations notwithstanding, his email prompted me to ask myself, "*Why would someone go to the trouble of developing and applying a three-phase model when the CYCLOPS framework gets it mostly right?*" The answer that occurred to me was, "*The liquid layer is probably where ballistic modifiers work their magic*." To wit, a small (<5 wt%) quantity of a compound/catalyst with the capacity to significantly impact $r(P)$ will be added to optimize a rocket propulsion system's performance, with a specific objective often being to minimize (in a pressure range of interest) the exponent (n) in the Vielle's burning-rate law,

$$r = AP^n \tag{1}$$

where A is constant. Shown schematically in Figure 1, the region of the $r(P)$ plot in which n is minimized is often referred to as a "plateau." At pressures below which the plateau occurs, n's value is considerably greater than the value of n for the uncatalyzed/baseline formulation. This pressure range is referred to as the "super-rate" region.

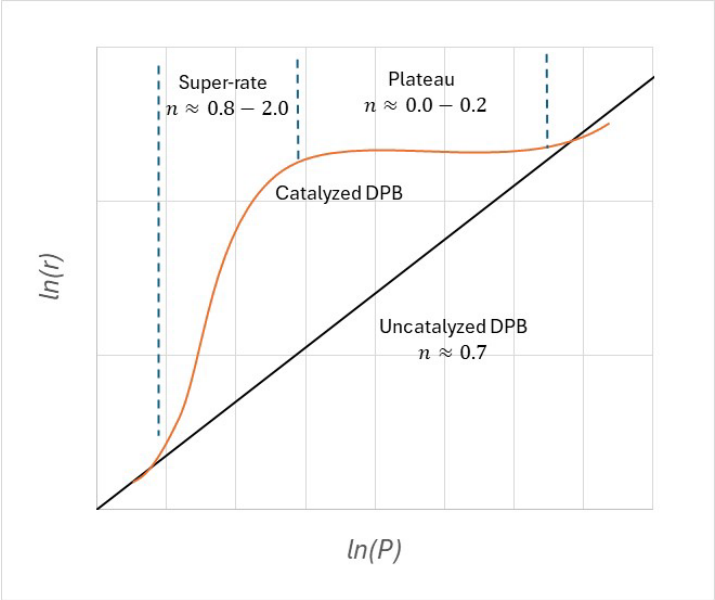

Figure 1. Schematic depiction of super-rate and plateau burning-rate regions. Adapted from Kubota et al. (1974).

In the case of double-base propellants (DBPs), whose primary ingredients are the nitrate esters nitrocellulose (NC) and nitroglycerine (NG), current standard modifiers for producing plateaus are lead (Pb)-based compounds (Warren et al. 2021). Unfortunately, such compounds pose considerable risks to human health and the environment and alternatives have long been sought. Toward guiding that search, various theories have been proposed to explain how modifiers impact the deflagration process. Warren et al. (2021) reviewed four of them: photochemistry (Camp et al. 1980), chelation/complex-formation (Dauerman and Tajima 1968; Suh et al. 1974; Fifer and Lannon 1975; Farber and Srivastava 1978), carbon–soot formation (Kubota et al. 1975), and free-radical generation (Sinha and Patwardhan 1968). All posit mechanisms that change the combustion chemistry to produce a super-rate. However, Warren et al. (2021) concluded that only Kubota et al.'s carbon–soot formation theory can also explain plateau burning.

My speculation that ballistic modifiers performed their function in the liquid layer was based (primarily) on findings produced by CYCLOPS-based modeling studies. Particularly influential was a study designed to test a hypothesis Dr. William

Anderson (DEVCOM Army Research Laboratory, retired) had surmised regarding the capacity of a small concentration of a modifier/additive to effect a non-negligible change in a nitrate-ester–based propellant's *gas-phase* combustion chemistry. Having previously found that reactions that were important determinants of the length of the dark-zone of flames produced by nitrate esters burning at low (<10 atm) pressures were also important determinants of their burning rates at higher pressures (Anderson et al. 2011), he thought the burning rates of gun and min-smoke rocket propellants might be significantly modified by introducing additives whose decomposition products would accelerate or decelerate the growth of the free-radical pool near the surface.

To test his hypothesis, the impacts on the burning rate of NG produced by the addition of seven different small molecules were predicted with a CYCLOPS-based model. It was found that there was no correlation between the burning rate predictions and the length of the dark zone at a given pressure, suggesting the impact of the additives on radical pool growth was not significant (Chen et al. 2019). Rather, the factor found to be most responsible for the difference in the burning-rate predictions produced by different additives was the additive's enthalpy of formation. In addition, the changes to the burning rates were small. Thus, I did not think that a modifier's impact on gas-phase combustion chemistry alone would be sufficient to produce burning-rate changes with magnitudes approaching those obtained by adding catalysts to DBPs.

Likewise, those results also suggested that a heterogeneous reaction at the liquid–gas interface would have limited potential to produce large burning-rate changes. Consistent with that suspicion, Miller (1997) found that the burning-rate predictions produced by his three-phase combustion model did not change with the introduction of a heterogeneous reaction.

Observing the limited potential of the modification of gas-phase combustion chemistry or chemistry at the burning surface (in isolation) to effect large burning-rate changes, the next logical place to look for an additive's potential impact on burning rates was in the liquid layer. Indeed, I could imagine how an additive-induced increase in the liquid-phase's (LP's) reaction rates, a lowering of its freezing point, or an increase in its boiling point might couple with a reduction in the LP's thickness as P increased to produce $r(P)$ profiles with super-rate and plateau regions. Thus, a three-phase model might provide insights that could accelerate the tailoring of propellants for developmental propulsion systems. However, at present, the modeling of reaction chemistry in condensed phases is very primitive (McQuaid et al. 2021). And, even if predictions from such models could be trusted, the cost and time required to develop, validate, and apply such models would be difficult to justify.

Based on those considerations, I thought a more practical first step toward examining my speculation would be to determine if it had the potential to produce catalyzed-DBP–like $r(P)$ profiles in a prototypical system, and Miller's three-phase model of the deflagration $O_{3,s}$ appeared suitable for that purpose. Unfortunately, there was not enough detail in his reports concerning the governing equations and numerical methods he incorporated into his model for me to simply recreate it, and I doubted I could find an archived copy of his program. Therefore, I formulated and programmed my own model, incorporating lessons learned from my development of CYCLOPS3_WPSB (McQuaid and Stone 2024). A major part of the effort was formulating a model of the LP's dynamics and developing a method for predicting the thickness of the liquid layer (d) that would satisfy specified boundary conditions. Summaries of those two aspects of the model are provided herein.

To validate the model's numerical methods, I tried to reproduce Miller's (1997) simulations. The agreement between the two models' $r(P)$ and $d(P)$ predictions was reasonable (but not as good as I thought they would be). However, a (minor) inconsistency in my model (and presumably Miller's) was discovered whose cost to resolve could not be justified. This, too, is discussed.

To test my hypothesis that the interplay between catalyst-induced changes in the LP's thermochemical kinetic properties could produce $r(P)$ profiles with both super-rate and plateau regions, the impact of heuristically specified changes to the LP's chemical kinetics mechanism and its species' thermochemical properties were calculated and assessed. Profiles with both super-rates and plateaus were achieved by 1) limiting the chemical kinetics mechanism to one reversible reaction for the decomposition of $O_{3,l}$ into O_l and $O_{2,l}$, and 2) changing the thermodynamic properties of O_l from a best guess. In addition, the capacity of those predicates to produce a super-rate and plateau could be further enhanced by decreasing the liquid-to-gas volatilization rate in proportion to $O_{3,l}$'s decomposition. The correspondence of these "mechanisms" and the theory positing complex formation as an explanation for super-rate burning is evident and discussed. Moreover, the model provides additional support for this theory by demonstrating it can concomitantly produce a plateau region.

2. The Three-Phase Model

A three-phase model requires that governing equations representing the continuities of mass and energy be formulated and solved for each phase and at the solid–liquid and liquid–gas interfaces. With each phase and interface posing challenges in their own right, based on my experience in developing and applying the (two-phase) CYCLOPS framework (McQuaid and Stone 2024), I thought it would be beyond

my capacity to establish efficient and reliable means for setting up and solving problems in which all the system's continuity equations were simultaneously coupled. Therefore, I decided to model the dynamics in each phase separately and employ an iterative procedure to get the conditions at the interfaces to match. (I believe Dr. Miller employed such a framework as well.) The subsections that follow summarize the protocol that I formulated and implemented to achieve that objective.

I also note that while in principle, the three phases could comprise any combination of phases in any order, in this study the phases were from left ($x = -\infty$) to right ($x = +\infty$) solid (s), liquid (l), and gas (g). Shown schematically in Figure 2, that order is assumed in the discussion that follows. As indicated in the figure, the boundaries between the phases corresponded to layers with infinitesimally small thicknesses within which the phase transitions occurred. In addition, the solid-phase's dynamics were not explicitly modeled.

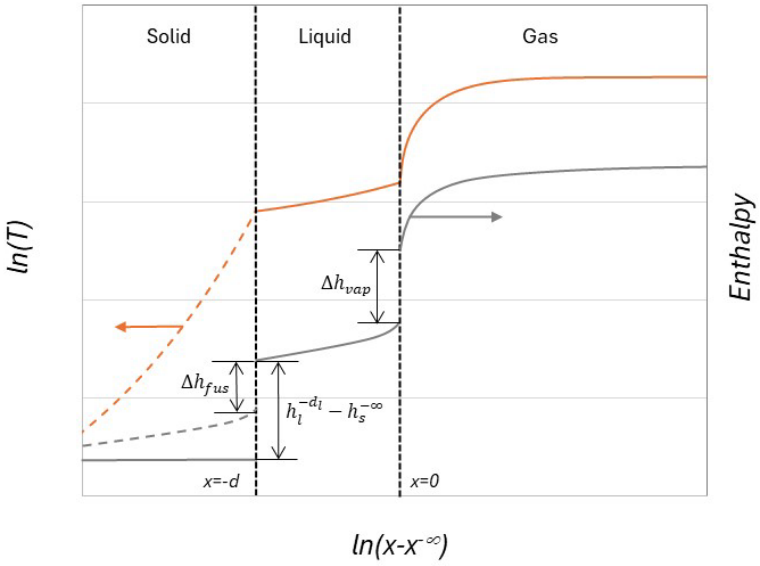

Figure 2. Three-phase model conceptualization. (Dashed lines are not explicitly modeled.)

2.1 The Gas-Phase Domain: $x \geq +0$

The gas-phase's dynamics were modeled with a precommercial CHEMKIN-III version of PREMIX. (The commercial version is summarized by Kee et al. [2000]). The governing equations it implements to conserve mass, energy, and species in a steady, isobaric, quasi-1D flame are presented and discussed by Kee et al. (1989). (Momentum conservation is implicitly satisfied if the governing equations for mass, energy, and species conservation are satisfied.)

The chemical kinetics mechanism and associated thermochemical and transport property data developed and specified by Miller (1995) were employed for this domain. The reactions in the mechanism along with some of their defining characteristics are shown in Table 1. The prescriptions employed to compute the species' thermochemical and transport properties are provided in the Appendix.

Table 1. Gas-phase reactions and some of their defining characteristics.[a]

Reaction		*A*	*b*	E_a cal/mol	$\Delta H_r(298K)$ cal/mol
R1	$O_{3,g}\ (+M) <=> O_g + O_{2,g}\ (+M)$	7.60E+12	0.0	24,500	+25.6
R2	$O_g + O_{3,g} <=> O_{2,g} + O_{2,g}$	1.14E+13	0.0	4570	–93.4
R3	$O_g + O_g + M <=> O_{2,g} + M$	1.38E+18	–1.0	340	–119.1

[a] Forward reaction rate coefficients were computed per $k^{rxn} = AT^b exp\left(\frac{-E_a}{RT}\right)$, where the units of A comprise mole-cm-sec-K as appropriate and R is the universal gas constant.

2.2 The Liquid–Gas Interface: $x = 0$

Given the CYCLOPS framework's proclivity for producing $r(P)$ values that were in reasonable agreement with measured values, I considered it would likely provide good initial estimates for the mass and energy fluxes at the liquid–gas interface and the interface's temperature (T^0). Therefore, I employed it as the starting point for the protocol.

The CYCLOPS framework is discussed in more detail elsewhere (Miller and Anderson 2000, 2004; McQuaid and Stone 2024). Briefly, Miller and Anderson (2000) showed that the 1D energy flux boundary condition at a planar interface between two phases in a spatial coordinate system (x) that moves at (burning rate) r relative to a spaced-fixed coordinate system reduces to

$$r\rho_s\left(\sum_k^K Y_{k,g}^{-0} h_{k,g}^{+0} - h_s^{-\infty}\right) = \left[\lambda_g \frac{dT}{dx}\right]^{+0} \tag{2}$$

where the left-hand side corresponds to the energy flux needed to raise the mass-specific enthalpy of a mass flux with density ρ_s from the value for the condensed phase at $x = -\infty$ ($h_s^{-\infty}$) to that of a set of nascent gas-phase products (K) at the interface ($x = 0$) with species (k) having mass fractions $Y_{k,g}$ and mass-specific enthalpies $h_{k,g}$. The right-hand side corresponds to the energy flux incident on the interface due to the thermal conductivity (λ_g) and temperature gradient (dT/dx) on the gas-phase side of the interface ($x = +0$). The parameters λ_g, dT/dx, and $h_{k,g}$ depend on T^0. The parameters λ_g and dT/dx also depend on P. It should be appreciated that this formulation of the energy conservation equation at $x = 0$ is

completely independent of the properties of the LP. That dependence is included via the LP model outlined in Section 2.3.

Miller's (and therefore this study's) specification for ρ_s (1.728 g/cm^3) was based on a measured value (Streng 1961) and was assumed to be independent of temperature. The $h_s^{-\infty}$ value for $O_{3,l}$ was computed based on Miller's prescription for the property. (Details of that prescription are provided in the Appendix.) I note that it produced a h_s value at 80 K that was approximately 2.5 kcal/mol higher than a value "mentioned" by Streng and Grosse (1959). From the standpoint of this study's objectives, that discrepancy was considered ignorable.

Per the conservation of mass,

$$\dot{M} = r\rho_s A_s = u_l \rho_l A_l = u_g \rho_g A_g \tag{3}$$

where $\dot{M}$ is the (x-independent) mass flow rate (in g/s), A_s is the solid's cross-sectional area, u_g (u_l) is the speed of the gas (liquid), ρ_g (ρ_l) is the gas's (liquid's) density, and A_g (A_l) is the gas's (liquid's) cross-sectional area.

As in Miller's (1997) model, an HLK representation was employed to calculate the volatilizing mass flux ($\dot{m}_{l\to g}$) at the interface. Establishing a one-to-one mapping between the liquid-phase species (k') and the gas-phase species (k) at $x = -0$, viz.,

$$k' = k \tag{4a}$$

$$X_{k',l}^{-0} = X_{k,g}^{-0}, \tag{4b}$$

it was,

$$\dot{m}_{l\to g} = \dot{M}/A_s = \textstyle\sum_k^K (W_k/2\pi RT^0)^{\frac{1}{2}} \left(X_{k,g}^{-0} P_{sat}^0 - X_{k,g}^{+0} P\right) \tag{5}$$

where the W_k are the species' molecular weights, R is the universal gas constant, $X_{k,g}^{-0}$ and $X_{k,g}^{+0}$ are the species' mole fractions on the liquid and gas-phase sides of the interface, respectively, P_{sat}^0 is the saturated (equilibrium) vapor pressure of the chemical composition at the interface, and P is the system's (constant) pressure. I did not include a heterogenous reaction at the interface that Miller included in his model. He found that it had effectively no impact on burning-rate predictions. Therefore, with respect to this study's objectives, his results addressed that issue and including a heterogenous reaction in my model was considered unnecessary.

For four of the five cases presented herein, an estimate for P_{sat}^0 was calculated by (purposely) neglecting O_l's and $O_{2,l}$'s contributions to P_{sat}^0. Derived from measured $P_{sat}(T)$ data for pure $O_{3,l}$ (Stull 1947), the prescription was,

$$\frac{P_{sat}^{0}}{1\ \mathrm{dyn/cm^2}} = 8.517\mathrm{x}10^{9}\exp\left(\frac{-1463}{T}\right) \tag{6a}$$

where T is in Kelvin. To explore the impact of raising or lowering P_{sat}^{0} in proportion to the concentrations of the decomposition products at $x = -0$, in the fifth case it was computed per

$$\frac{P_{sat}^{0}}{1\ \mathrm{dyn/cm^2}} = 8.517\mathrm{x}10^{9}\exp\left(\frac{-1463}{T}\right) + cX_{O_{2,l}}^{-0}1.487\mathrm{x}10^{10}\exp\left(\frac{-871.6}{T}\right) \tag{6b}$$

where c was a heuristically specified constant and the other coefficients in the second term on the right-hand side were derived from measured values for $O_{2,l}$. (Regardless of whether this might be a reasonable representation for mixtures of O_l, $O_{2,l}$, and $O_{3,l}$, the objective was to change the P_{sat}^{0} value for pure $O_{3,l}$ via a term whose parameterization was physically grounded.)

For the first iteration ($n' = 1$), $X_{O_{3,l/g}}^{-0}$ was set equal to 1. For subsequent iterations, the $\left\{X_{k,l/g}^{-0}\right\}$ were specified based on the results produced by the LP model outlined in Section 2.3. The procedure for finding the T^0 and $\dot{M}$ (and thereby, r) values at which Equations 2 and 5 were satisfied is summarized elsewhere (McQuaid and Stone 2024).

2.3 The Liquid Layer: $-d < x \leq -0$

To simulate the liquid layer's dynamics, governing equations and boundary conditions analogous to those employed to model the gas-phase domain were formulated and an in-house precommercial CHEMKIN-III version of PREMIX was modified to set up and solve them. (Miller [1997] indicates he also used a modified version of PREMIX for this purpose.)

For the energy conservation equation, I assumed the term accounting for diffusion would be negligibly small and zeroed it. (I was also concerned that PREMIX's subroutines for computing diffusion coefficients were specifically designed and parameterized for gas-phase systems and thus might produce compromisingly poor estimates for a condensed phase.) That left,

$$\dot{M}\frac{dT}{dx} - \frac{1}{c_{p,l}}\frac{d}{dx}\left(\lambda_l A_l \frac{dT}{dx}\right) + \frac{A_l}{c_{p,l}}\sum_{k'=1}^{K}\dot{\omega}_{k',l}\,h_{k',l}W_{k'} = 0, \tag{7}$$

where $c_{p,l}$ was the liquid's heat capacity, λ_l was its thermal conductivity, $\dot{\omega}_{k',l}$ was the molar rate of production of species k' per unit volume, and $h_{k',l}$ was its mass-specific enthalpy.

Likewise, the term accounting for diffusion was zeroed in the species conservation equations, leaving,

$$\dot{M}\frac{dY_{k',l}}{dx} - A_l\dot{\omega}_{k',l}W_{k'} = 0, \tag{8}$$

where $Y_{k',l}$ was the mass fraction of k'.

Based on the assumption that λ_l, and ρ_l values would be insensitive to the extent of $O_{3,l}$'s decomposition (up to the limit it was allowed in the study), estimates for them were calculated via formulae derived from measured data. They were, respectively,

$$\frac{\rho_l}{1\ \mathrm{g/cm^3}} = (0.551 + 6.25x10^{-4}T + 3.35x10^{-6}T^2)^{-1} \tag{9}$$

where T is in K (Brabets and McDonough 1957), and

$$\frac{\lambda_l}{1\ \mathrm{cal/cm-K-s}} = 4.999\mathrm{x}10^{-4} + 3.652\ \mathrm{x}10^{-7}T \tag{10}$$

(Waterman et al. 1958).

As stated in the introduction, heuristic variations of the gas-phase chemical kinetics mechanism were specified to represent the decomposition of $O_{3,l}$. The results produced by five different mechanisms are presented herein. Their reactions, the parameterizations of those reactions' rate coefficients, and their association with the five cases for which results are presented in Section 3 are provided in Table 2.

Table 2. Liquid-phase chemical kinetics mechanisms.[a]

Case	Label	Reaction	*A*	*b*	E_a cal/mol
Case 2[b]	R1-C2	$O_{3,l}(+M)$ <=> O_l+ $O_{2,l}$ $(+M)$	7.60E+12	0.0	24,500
	R2-C2	O_l+$O_{3,l}$ <=> $O_{2,l}$+$O_{2,l}$	1.14E+13	0.0	4570
	R3-C2	O_g+O_g+M <=> $O_{2,g}$+M	1.38E+18	–1.0	340
Case 3a	R1-C3a	$O_{3,l}$ => $O_{2,l}$+O_l	2.50E+01	0.0	0.0
Case 3b	R1-C3b	$O_{3,l}$ => $O_{2,l}$+O_l	3.00E+05	0.0	2450
Case 3c	R1-C3c	$O_{3,l}$ => $O_{2,l}$+O_l	1.50E+09	0.0	4900
Cases 4 and 5	R1-C4	$O_{3,l}$ <=> $O_{2,l}$+O_l	4.00E+13	0.0	7500

[a] Reaction rate coefficients were computed per $k^{rxn} = AT^b exp\left(\frac{-E_a}{RT}\right)$, where the units of A comprise mole-cm-sec-K as appropriate and R is the universal gas constant.

[b] The liquid-phase mechanism for Case 2 was identical to the gas-phase mechanism (Table 1).

For the mechanism specified for Case 2, the computation of rates for R1-C2 and R3-C3, which are a function of the concentration of third bodies (M), involved converting ρ_l into an "effective" pressure (P_l) per

$$P_l = \frac{\rho_l RT}{\bar{W}_l} \tag{11}$$

where $\bar{W}_l$ was the mean molecular weight of the liquid.*

The enthalpy ($h_{O_3,l}$) and heat capacity ($c_{p,O_3 l}$) of $O_{3,l}$ as a function of temperature were computed using the formulae prescribed by Miller (1995). Those prescriptions are provided in the Appendix. Figure 3 shows the $h_{O_3,l}(T)$ values computed on that basis, comparing them to $h_{O_3,g}(T)$ values. I verified that Miller's prescription for computing $c_{p,O_3 l}$ reproduced values generated by a formula Brabets and Waterman (1958) derived from values they measured. I did note that Brabets and Waterman considered their formula "sufficiently accurate for engineering calculations over the temperature range of 90 K to 150 K." Given that O_3's critical temperature is 260 K, this formula's validity will certainly degrade as temperatures approach 260 K and be invalid above that limit. However, to the extent the system was merely of interest as a prototype for a DBP and the impact of approaching (and exceeding) the critical point of the chemical composition at the liquid–gas interface of a deflagrating DBP was not something I was hoping to model and assess, that issue was not relevant.

* Appreciating that this was not a theoretically sound basis for computing the rates of these reactions in a condensed phase (McQuaid et al. 2021), I nonetheless employed it because, to the extent my objective was to study the interplay between LP reaction rates and burning rates and $k_{i,l}^{rxn}$ values were to be heuristically specified to achieve that end, it was adequate for that purpose.

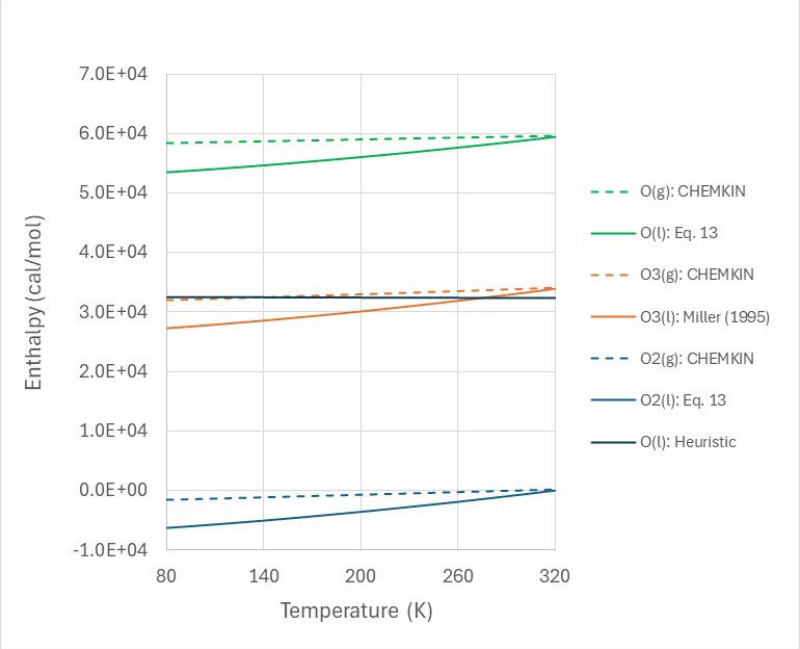

Figure 3. Comparison of the enthalpies of gas- and liquid-phase *O*, O_2, and O_3 as a function of temperature.

I also note that, similar to the situation found in the solid phase, the $h_{O_3,l}(90)$ value computed using Miller's formula was approximately 2.4 kcal/mol lower than a value published by Streng and Grosse (1959). Neither Miller nor Streng and Gross provided all the information that was needed to derive the values they published. Trusting Dr. Miller's work and wanting my model to be as similar to his as possible, I used his prescription.

The enthalpies of O_l and $O_{2,l}$ were estimated based on my assumption that at a given temperature the difference between their $h_{k,l}$ values and $h_{O_3,l}$'s would be the same as the difference between their $h_{k,g}$ value and $h_{O_3,g}$'s, viz.,

$$h_{k,l}(T) = h_{k,g}(T) - \left(h_{O_3,g}(T) - h_{O_3,l}(T)\right). \tag{12}$$

Polynomials were fit to the $h_{k,l}(T)$ plots generated by Equation 12 and converted to standard CHEMKIN functional form for integration into the program. Comparisons of the $h_{k,l}$ and $h_{k,g}$ values produced by this approach are shown for the temperature range of interest in Figure 3.

Regarding the validity of the $h_{k,l}(T)$ estimates generated by Equation 12, I noted that $h_{k,g}(T)$ was greater than $h_{k,l}(T)$ for all T in the range of interest. As such, they were at least physically plausible and therefore adequate for exploratory sets of calculations. As will be discussed, I subsequently modified the coefficients employed to compute $h_{O,l}$ so that a $Y_{O_3,l}$ value of approximately 0.9 would be

reached at $x = -0$ in a 1-atm simulation. The prescription for that case is provided in the Appendix.

In addition to estimating $h_{k,l}$ values, estimates for the species' entropies ($S_{k,l}$) were needed for simulations in which $\dot{\omega}_{k',l}$ values were calculated. Because Miller (apparently) did not attempt to model chemical reactivity in the LP, his effort offered no guidance with respect to this matter. Noting that it simply required specifying the seventh (a_7) of seven coefficients employed to compute a species' thermodynamic properties, and that the value of a_7 for liquid water was approximately half that of gaseous water, I specified a_7 in the formulae for computing $S_{k',l}$ to be half that of its gas-phase counterpart. They are provided in the Appendix.

The boundary condition for the LP side of the solid–liquid interface ($x = -d_l$) was,

$$T^{-d_l} = T_m \tag{13}$$

where T_m was $O_{3,s}$'s melting point. Following Miller (1997), I set it equal to 80 K.

For the LP side of the liquid–gas interface ($x = -0$), the boundary conditions were,

$$T^{-0} = T^{+0} \tag{14}$$

$$\left[\lambda_l \frac{dT}{dx}\right]^{-0} + \frac{\dot{M}}{A^0_{l/g}}\left[\sum_k^K h_{k,g} - \sum_{k'}^K h_{k',l}\right]^0 = \left[\lambda_g \frac{dT}{dx}\right]^{+0} \tag{15}$$

where the values of T^{+0} and $\left[\lambda_g \frac{dT}{dx}\right]^{+0}$ were set equal to values produced by the preceding CYCLOPS-based step.

To find the value of d that would bring the right- and left-hand sides of Equation 15 into agreement, an initial guess for it was made on the basis of the target $\left[\lambda_l \frac{dT}{dx}\right]^{-0}$ value and the $\left[\lambda_l \frac{dT}{dx}\right]^{-d_l}$ value satisfying

$$\frac{\dot{M}}{A_s}\left(h_l^{-d_l} - h_s^{-\infty}\right) = \left[\lambda_l \frac{dT}{dx}\right]^{-d_l}. \tag{16}$$

Observing the proportionality between d and $\left[\lambda_l \frac{dT}{dx}\right]^{-0}$, the value of d for the next iteration ($n' + 1$) was estimated per

$$d_{n'+1} = d_{n'}\left[\frac{\left[\lambda_l \frac{dT}{dx}\right]^{-0}_{n'}}{\left[\lambda_l \frac{dT}{dx}\right]^{-0}_{target}}\right]. \tag{17}$$

That procedure was repeated until

$$\left| 1 - \frac{\left[\lambda_l \frac{dT}{dx}\right]^{-0}_{n'}}{\left[\lambda_l \frac{dT}{dx}\right]^{-0}_{target}} \right| \leq 0.001. \tag{18}$$

The chemical composition of the liquid at $x = -0$, i.e., $\{X_{k,l}^{-0}\}$, was then employed as $\{X_{k.g}^{-0}\}$ for a subsequent CYCLOPS step. The three-phase problem as a whole was considered solved when the difference between the $\dot{M}$ values predicted by two successive CYCLOPS steps was less than 0.1%.

2.4 The Solid Layer: $-\infty < x \leq -d$

Although Miller discussed modeling the dynamics of the solid phase, he did not present results for it and he did not discuss how those dynamics influenced the burning-rate predictions. I assume that was because their impact was negligible. Indeed, upon trying to reproduce his study, I concluded that (using the model as formulated) a nonreactive phase could not significantly change the r predictions for the system. Therefore, I did not explicitly model it; limiting to ρ_s and $h_s^{-\infty}(T)$ the properties of the solid phase that had to be specified to perform the calculations. As discussed in Section 2.2, ρ_s was set equal to 1.728 g/cm^3, and $h_s^{-\infty}(T)$ was computed with the formula Miller employed for that purpose. The latter is provided in the Appendix. Consistent with Miller's study, the temperature at $x = -\infty$ was set equal to 40 K.

3. Results

Starting with a case that mirrored the one presented and discussed by Miller (1995, 1997), a sequence of cases whose formulations were based on lessons learned from the case that preceded it ultimately led to a case in which an $r(P)$ plot with both super-rate and plateau regions was produced. Instructive as to the changes a catalyst would have to induce in the LP's thermochemical kinetic properties to produce the desired behavior, they are presented case-by-case in the order they were constructed and analyzed.

3.1 Case 1: No LP Reactions; Best-Guess LP Thermodynamic Properties

To determine if my model would produce the same results as Miller's if it employed the same inputs, I tried to reproduce his primary case. Referred to hereafter as Case 1, the model's formulation was predicated on chemical reactivity and

diffusivity in the solid and liquid phases being negligible. In my model, this case was implemented by zeroing the $\dot{\omega}_{k,l}$ values in Equations 7 and 8.

Figure 4 compares the $r(P)$ and $d(P)$ predictions produced by the two models. As shown, their $r(P)$ predictions were nearly identical (as expected). Relevant to establishing expectations for mechanistic changes to produce super-rate and plateau burning-rate regions in subsequent cases, the r prediction at 10 atm (2.5 cm/s) is more than 1 order of magnitude higher than that of a "typical" uncatalyzed DBP burning at the same pressure. (See, e.g., Kubota et al. [1974]). In addition (and as noted by Miller) the pressure dependence was well approximated by Equation 1, with a fit of it to the predictions yielding $n \approx 1$. This value is considerably higher than those of uncatalyzed DBPs. As such, it was appreciated that mechanistic changes were unlikely to produce burning-rate changes with magnitudes approaching those produced by adding catalysts to DBPs, tempering expectations.

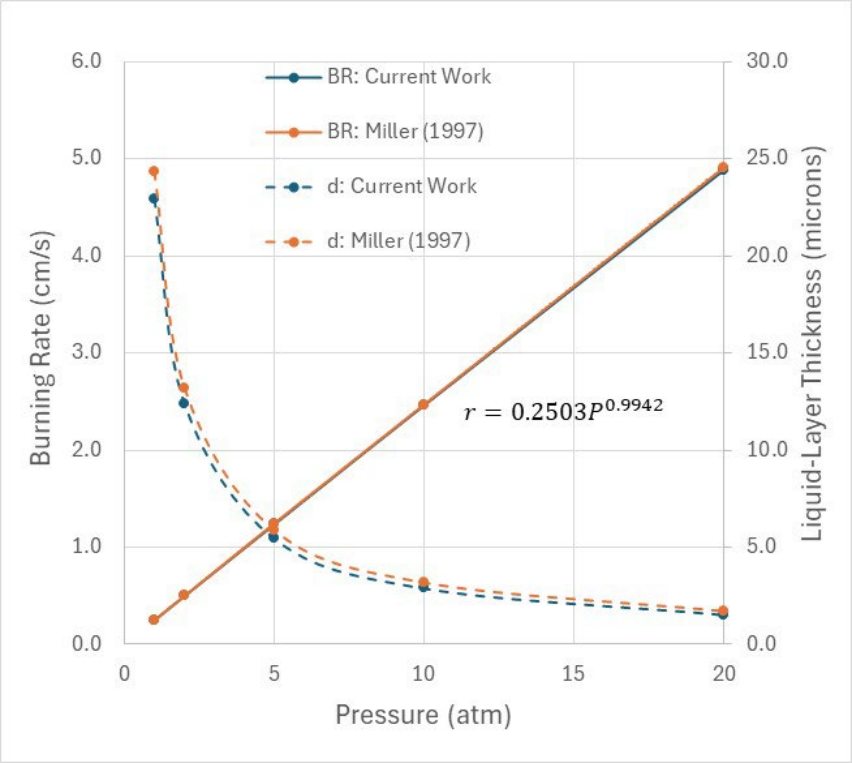

Figure 4. Comparisons of predictions for Case 1: Current work vs. Miller (1997).

The differences between the two models' $d(P)$ predictions were slightly larger. The value generated by my model was about 6% shorter at 1 atm and the differences gradually increased with pressure. At 20 atm, my model's result was approximately 14% shorter than Miller's. (Not shown, the differences between the two models' predictions for T^0 were slightly less than that.)

Having observed the sensitivity of CYCLOPS-based predictions to specifications such as the convergence criteria employed for the PREMIX calculations and the method for calculating the temperature gradient at the liquid–gas interface, all of which could well have been different between my model and Miller's,* I was satisfied with the agreement. However, some results produced by my model raised concerns. For one, based on Miller's reports and my experience using the CYCLOPS framework, I assumed at the start of the effort that solutions that simultaneously satisfied Equations 13–16 could be found for a given $\dot{M}$ simply by varying d. Therefore, I attempted to simulate the LP's dynamics with the temperatures and temperature gradients at its bounding interfaces—namely, T^{-d}, T^{0}, $[dT/dx]^{-d_l}$, and $[dT/dx]^{-0}$—fixed at values calculated per those equations. However, those simulations invariably failed.

I assume they failed because T^{-d}, T^{0}, $[dT/dx]^{-d_l}$, and $[dT/dx]^{-0}$ are not completely independent of one another. Coupled via the physical properties of the liquid phase, for a given $\dot{M}$ and d, the specification of three of them produces a well-defined solution for the fourth. Therefore, it was clear that one or more of the constraints represented by Equations 13–16 would have to be relaxed.

Considering T^{-d}, T^{0}, and $[dT/dx]^{-0}$ values established via Equations 13–15 to be ground truths, I decided to completely eliminate the constraint on $[dT/dx]^{-d_l}$ imposed by Equation 16. With that constraint eliminated, converged solutions for a given d and $\dot{M}$ were readily obtained, and the search algorithm was able to find a d at a given $\dot{M}$ that would yield a solution that satisfied Equations 13–15. However, Equation 16 was not concomitantly satisfied to the same degree of accuracy. As shown in Figure 5, model-produced $[dT/dx]^{-d_l}$ values were invariably higher than values based on Equation 16.

* One notable difference between the two models I was able to discern based on Miller's report was the number of grid points discretizing the gas-phase domain. He reported that the results he presented were derived from simulations comprising ~4500 grid points. Employing PREMIX's (standard) grid refinement technique, my model could produce simulations meeting what I considered fairly tight convergence criteria with grids containing <100 points.

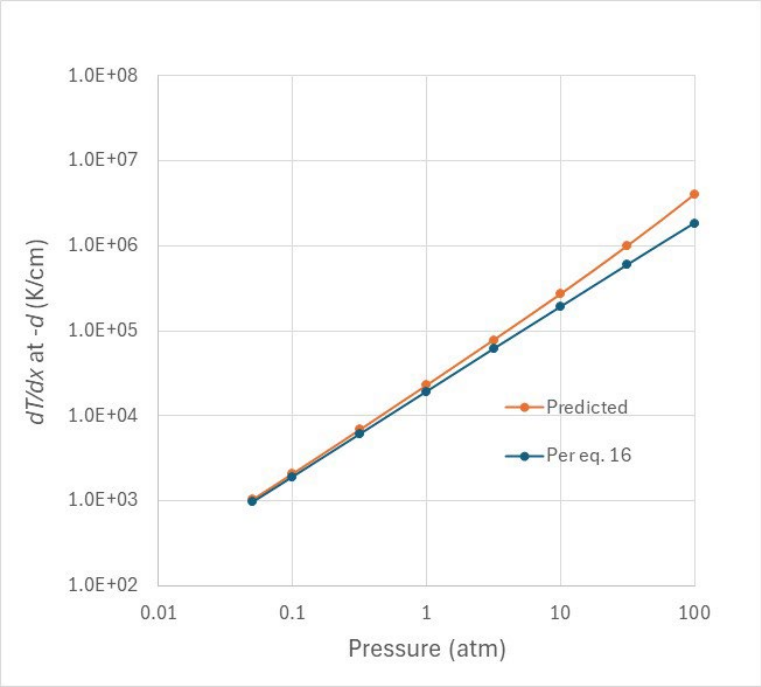

Figure 5. Comparison of model-based $[dT/dx]^{-d_l}$ predictions with predictions based on Equation 16.

Given the coupling between the four parameters, I assumed that better agreement between the predicted and target $[dT/dx]^{-d}$ values could only be achieved by including more physically realistic representations for the phase transitions, adding a term to represent diffusivity in the LP, or "refining" (the already approximate) thermochemical kinetic and transport property estimates for the species in one or more of the phases. And even then, it seemed likely I would have had to introduce a least-squares fitting procedure to find the values of $\dot{M}$ and d that would minimize the residuals for $[dT/dx]^{-d_s}$, $[dT/dx]^{-d_l}$, $[dT/dx]^{-0}$, T^0, and $[dT/dx]^{+0}$.

Since the time and cost necessary to develop, implement, and validate such changes would have been far greater than could be justified, the question became whether the model's shortcomings would compromise my capacity to draw reliable conclusions about the potential for processes in the liquid layer to produce super-rate and plateau burning. I concluded they would not. For one, within the pressure range studied by Miller (1–20 atm) the discrepancies were relatively small and as already noted might have been due to differences in the models' numerical methods (not their physics). In addition, since I was specifying parameters of the LP model to achieve targeted values for $X_{O_l}^{-0}$ and $X_{O_{2,l}}^{-0}$ at one P and comparing values produced at other P's to them, the primary requirement was that, for a given set of input parameters, the model produce $X_{O_l}^{-0}$ and $X_{O_{2,l}}^{-0}$ predictions relative to the standard that were consistent within the pressure range considered. Finding that the

trend shown in Figure 5 occurred in every case considered, I concluded it would meet that requirement.

3.2 Case 2: LP Mechanism = GP Mechanism; Best-Guess LP Thermodynamic Properties

Having previously theorized that for a given chemical composition, the reactions that were important in a condensed-phase system would be the same as those in a gas-phase system (McQuaid et al. 2021), I integrated into the LP model a chemical kinetics mechanism with the same three reactions and $k_{i,f}^{rxn}$ parameterizations as those in the gas-phase mechanism. The thermodynamic properties of O_l and $O_{2,l}$ were estimated as described in Section 2.3. Consistent with expectations, the r, T^0, and d predictions were negligibly different from those produced for Case 1 (and thus are not shown). The $X_{O_l}^{-0}$ and $X_{O_{2,l}}^{-0}$ values were significantly lower than 10^{-12}, and thus not meaningful.

To confirm my speculation that $X_{O_l}^{-0}$ and $X_{O_{2,l}}^{-0}$ were negligibly small because the reverse rate coefficient for R1-C2 ($k_{R1-C2,r}^{rxn}$) was much greater than R1-C2's forward rate coefficient ($k_{R1-C2,f}^{rxn}$), I had the model output them (along with the rate coefficients for the other reactions). Representative values are shown in Table 3. Consistent with expectations, $k_{R1-C2,f}^{rxn}$'s value, which dictated the rate of $O_{3,l}$'s decomposition, was negligibly small (relative to the time scale of interest) and many orders of magnitude less than $k_{R1-C2,r}^{rxn}$.

Table 3. Forward and reverse rate coefficients for reactions in the LP mechanism: Case 2 (1 atm).

x	T (K)	Reaction	$k_{i,f}^{rxn}$	$k_{i,r}^{rxn}$
		R1-C2	1.2E–52	6.0E–09
$-d$	82.6	R2-C2	9.3E+00	0.0
		R3-C2	2.1E+15	0.0
		R1-C2	3.0E–22	9.2E–04
-0	155.6	R2-C2	4.4E+06	0.0
		R3-C3	3.0E+15	0.0

3.3 Case 3: Irreversible, One-Step LP Mechanism; Best-Guess LP Thermodynamic Properties

I assumed that to effect a significant change in the burning rate, the decomposition of $O_{3,l}$ would have to produce a non-negligible $X_{O_l}^{-0}$ value, and the Case 2 results made clear that to produce such a value, $k_{R1,f}^{rxn}$'s value would have to be significantly raised both in absolute terms and relative to $k_{R1,r}^{rxn}$, $k_{R2,f}^{rxn}$, and $k_{R3,f}^{rxn}$. Given that my best guess for the enthalpies of O_l, $O_{2,l}$, and $O_{3,l}$ would always yield $k_{R1,r}^{rxn} > k_{R1,f}^{rxn}$,

but curious as to whether the model could produce $r(P)$ plots with both super-rate and plateau regions without modifying O_l's or $O_{2,l}$'s thermodynamic properties, I specified a mechanism that comprised one irreversible step:

$$O_{3,l} => O_l + O_{2,l}, \qquad \text{(R1-C3)}$$

and by trial and error, sought (A, E_a) pairs (with b = 0) for parameterizing $k^{rxn}_{R1-C3,f}$ that would produce a $Y^{-0}_{O_{3,l}}$ value of approximately 0.95 in a 2-atm simulation. Combinations that produced such a result included (34.0, 0.0), (3.0×10^5, 2450), and (1.5×10^9, 4900). In the discussion that follows, they are referred to as Cases 3a, 3b, and 3c, respectively.

The values of $X^{-0}_{O_l}$ and $X^{-0}_{O_{2,l}}$ along with the fractional increases in r that those cases produced relative to Case 1 (i.e., no LP chemical reactivity) are shown as a function of P in Figure 6. Notably, the fractional increases in the burning rates essentially mirrored increases in $X^{-0}_{O_l}$ values with decrease in P until $X^{-0}_{O_l}$ and $X^{-0}_{O_{2,l}}$ predictions exceeded about 0.07. At that point the calculations failed because the boundary conditions represented by Equations 13–15 could only be met if the temperature gradient at the solid–liquid interface was negative. Figure 6 also shows that, within the pressure range considered, the dependence of the change in the fractional burning-rate increase (FBRI) with respect to P decreased with increasing E_a: $E_a(Case\ 3c) > E_a(Case\ 3b) > E_a(Case\ 3a)$.

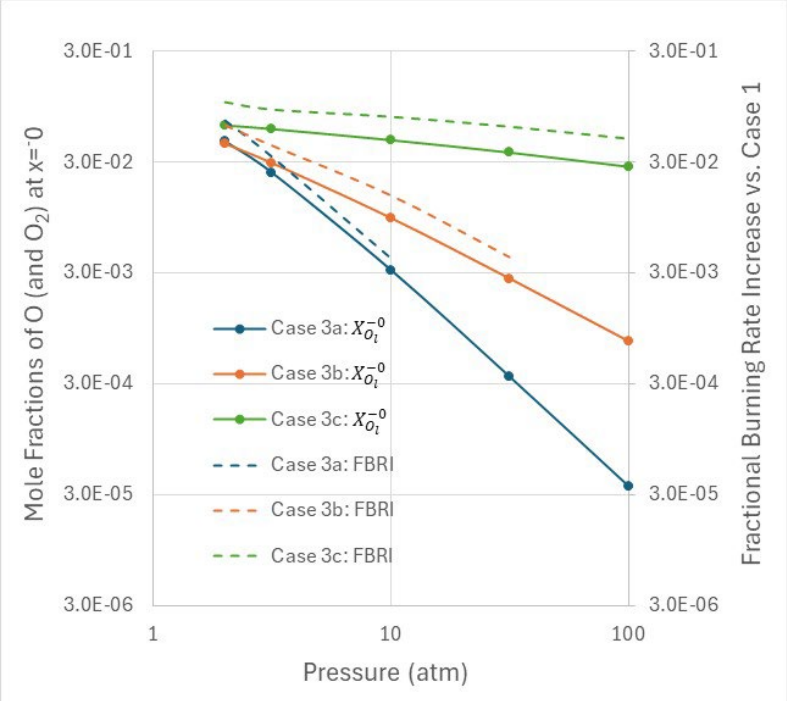

Figure 6. Case 3 results for $X^{-0}_{O_l}$ and FBRIs as a function of *P*.

The finding that the increases in the burning rates were directly proportional to the increases in $X_{O_l}^{-0}$ values was disappointing but not unexpected. (As already mentioned, the NG-additive study by Chen et al. [2019] indicated the limited ability of radical pool growth alone to increase burning rates.) It meant that to produce burning-rate changes with magnitudes similar to those produced by adding a Pb-based catalyst to a DBP, the targeted $Y_{O_{3,l}}^{-0}$ value would have to be much lower than 0.95, and that would be at odds with my expectations for the overall impact a catalyst could have on an LP's reaction chemistry. In an attempt to increase the burning rates relative to the amount of $O_{3,l}$ decomposed, I tested whether alternative $X_{O_l}^{-0}$:$X_{O_{2,l}}^{-0}$ ratios whose totals summed to 0.1 would produce larger burning-rate increases. However, (somewhat surprisingly) the 50:50 ratio produced by R1-C3 yielded the maximum.

The finding that the burning rates did not return to Case 1 values as the pressure decreased was somewhat surprising. I had expected that the presence of a barrier at the relatively low temperatures of the LP at lower system pressures would severely limit the rate of the reaction, and thus that an attendant drop in $X_{O_l}^{-0}$ and $X_{O_{2,l}}^{-0}$ values would be observed. That not being the case, I assumed that the relatively low rates of the reaction in the lower-pressure simulations were offset by the much longer residence time the material had in the LP due to the lower $\dot{M}$'s and the longer d's.

3.4 Case 4: Reversible, One-Step LP Mechanism; Heuristic LP Thermodynamic Properties

Because the burning rates did not return to Case 1 values as the pressure decreased for the irreversible, single-step reaction (R1-C3), I made it reversible,

$$O_{3,l} <=> O_l + O_{2,l}, \qquad \text{(R1-C4)}$$

and ran simulations with $k_{R1-C4,f}^{rxn}$ equal to each of the three $k_{R1-C3,f}^{rxn}$ parameterizations considered in Section 3.3 to see what would happen. In short, the results were effectively the same as Case 1. Despite the specified $k_{R1-C3,f}^{rxn}$ parameterizations increasing the forward rate relative to (the baseline) k_{R1-C2}^{rxn}, that benefit was more than offset by the reverse rate, which (deriving from the equilibrium constant for the reaction calculated based on my best guesses for the thermodynamic properties of O_l and $O_{2,l}$) was strongly favored. Therefore, I heuristically modified the parameterizations of both $k_{R1-C4,f}^{rxn}$ and $h_{O,l}$ until a simulation at 1 atm produced $X_{O_l}^{-0}$ and $X_{O_{2,l}}^{-0}$ values that were approximately equal to 0.11. This corresponded to $Y_{O_{3,l}}^{-0}$ equaling 0.88 (i.e., ~12 wt% of the starting $O_{3,l}$ decomposed within the LP). The parameterization of $k_{R1-C4,f}^{rxn}$ that produced this

result is shown in Table 2. The change in $h_{O,l}$ that produced it can be inferred from Figure 3.

The values of $X_{O_l}^{-0}$ (and therefore $X_{O_{2,l}}^{-0}$) along with the fractional increases in the burning rate that this case produced relative to Case 1 (i.e., no LP chemical reactivity) are shown as a function of P in Figure 7. As shown in Figure 8, the magnitudes of the changes in the burning rates were small compared to the magnitudes of the changes in the burning rates of DBPs that Pb-based catalysts are observed to produce. But as already noted, relative to DBPs, the magnitudes of $r(P)$ and n for the baseline O_3 system are extremely high and the potential for mechanistic changes to produce changes in $r(P)$ and n comparable to those observed for DBPs was limited. Therefore, I considered the $r(P)$ plot for Case 4 evidence that the mechanism implied by it had the potential to produce super-rate ($n > 1$) and plateau ($n < 1$) regions.

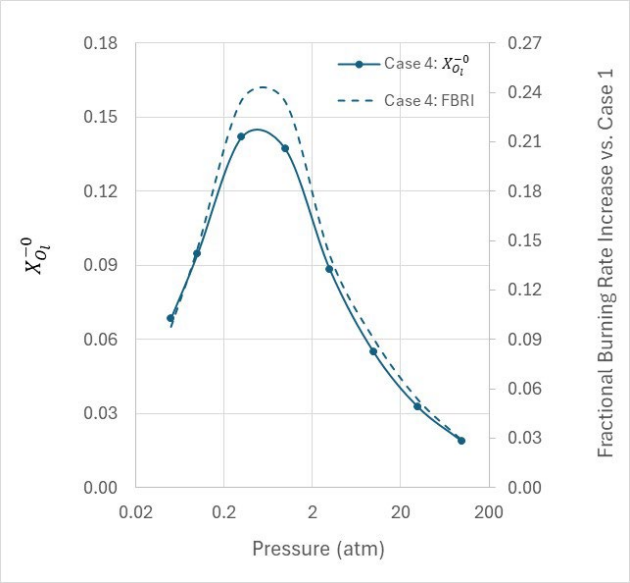

Figure 7. Case 4 results for $X_{O_l}^{-0}$ and FBRI as a function of *P*.

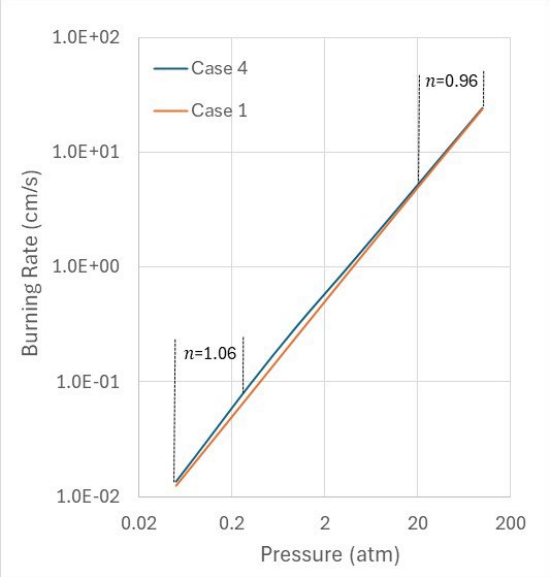

Figure 8. Comparison of Case 4 and Case 1 *r*(*P*) predictions.

3.5 Case 5: Reversible, One-Step LP Mechanism; Modified LP Thermo; Modified HLK

Having been able to specify a thermochemical kinetics mechanism that produced (at least qualitatively) an $r(P)$ plot with both super-rate and plateau $r(P)$ regions, but finding that the magnitude of the burning-rate changes produced by the changes to the LP's chemical kinetics mechanism alone were relatively small, I decided to determine if lowering or raising $P_{sat}(T)$ values as function of $X_{O_{2,l}}^{-0}$ (via Equation 6b) could amplify the changes. Although it is almost certainly the case that $P_{sat}(T)$ values for mixtures comprising O_l, $O_{2,l}$, and $O_{3,l}$ will be higher than that of pure $O_{3,l}$, I ran calculations corresponding to either possibility and found that to increase burning rates, $P_{sat}(T)$ values had to be lowered relative to those calculated per Equation 6a by specifying $c < 0$ in Equation 6b. Burning rates increased as c became more negative to the extent I allowed. Fractional differences between the $X_{O_l}^{-0}$ and r predictions produced when c was set equal to –0.008 are shown in Figure 9. Compared to Case 4, the modification to $P_{sat}(T)$ increased the $X_{O,l}^{-0}$ and r values at pressures less than 1 atm, producing an increase in n in the super-rate region.

Figure 10 shows the fractional change in T^0 wrought by the change to the HLK representation produced via the change in $P_{sat}(T)$ values. It reveals that lowering $P_{sat}(T)$ produced a higher temperature at the liquid–gas interface and that the effect became more pronounced as the pressure decreased. I assume this is why the maximum increases in $X_{O,l}^{-0}$ and r (relative to Case 1) occurred at a slightly lower pressure in Case 5 than they did in Case 4.

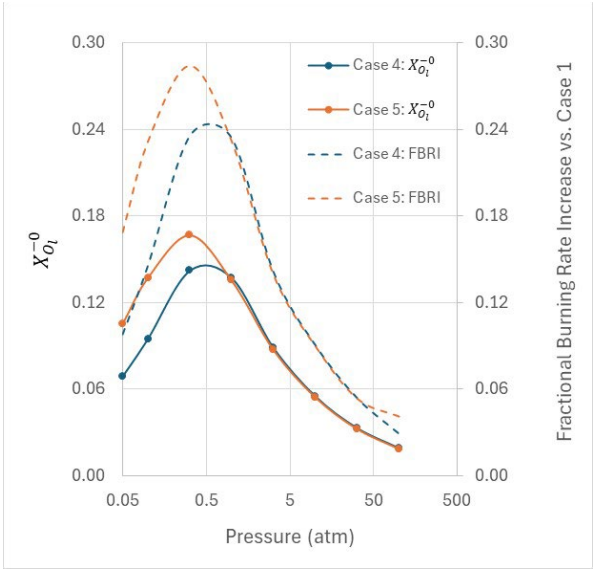

Figure 9. Comparison of Case 5 and Case 4 results for $X_{O_l}^{-0}$ and FBRIs as a function of *P*.

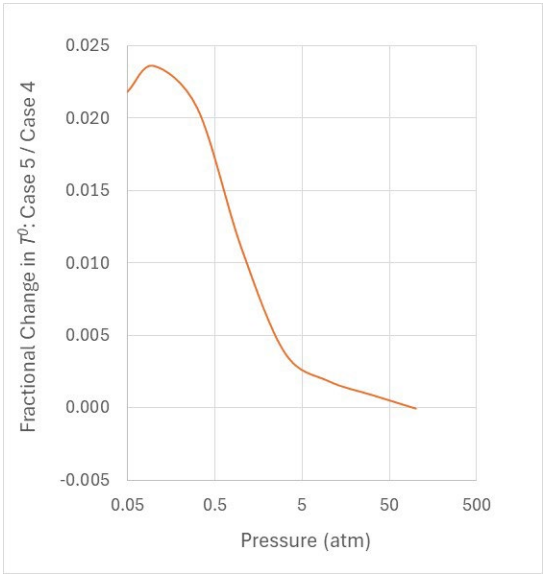

Figure 10. Fractional differences between Case 5 and Case 4 $T^0(P)$ values.

4. Discussion

It was not until the calculations whose results are summarized in Section 3 were complete that I became aware of published theories that had been proposed to explain super-rate and plateau burning-rate phenomena, learning about them in Warren et al.'s (2021) paper when I began to write this report. They were not a consideration in formulating the heuristically specified variations of the baseline model.

That being said, in formulating the variations, I tried to imagine a mechanism by which a catalyst (Pb_{cat}) might produce the changes I was specifying. Culminating in Case 5, those changes included the following:

- Reducing the barrier to the formation of O_l and $O_{2,l}$ from $O_{3,l}$
- Preventing O_l from further reacting
- Reducing O_l's enthalpy
- Reducing $P^0_{sat}(T)$ values in proportion to $X^{-0}_{O_2,l}$

The only mechanism I could think of that would produce all four changes was catalytic reduction of the activation energy (E_a) for $O_{3,l}$'s decomposition coupled with $O_2 \cdot Pb_{cat}$-O_l complex formation. That is, if instead of bestowing nonrealistic thermochemical kinetic properties on a system comprising only O_l, $O_{2,l}$, and $O_{3,l}$, including the E_a for R1, the thermodynamic properties of O_l, the capacity of O_l to subsequently react with O_l, $O_{2,l}$, or $O_{3,l}$, and the impact of $X^{-0}_{O_2,l}$ on P^0_{sat}, I could have produced the same effects by representing the LP's chemical kinetics with

$$O_{3,l} + Pb_{cat} \text{ <=> } (O \cdot Pb_{cat} \cdot O_2)_l \qquad \text{(R1-complex)}$$

where Pb_{cat} lowers the barrier to the dissociation of the $O - O_2$ bond in $O_{3,l}$ and binds the products until they reach the liquid–gas interface where they are spontaneously released. Beyond offering a physically plausible explanation for the lowering of the barrier to the decomposition of $O_{3,l}$, effectively lowering O_l's enthalpy, and preventing further reaction of O_l, I could imagine that $(O \cdot Pb_{cat} \cdot O_2)_l$ might also lower the mixture's $P^0_{sat}(T)$ values.

In essence, the R1-complex reaction corresponds to chelation/complex-formation theory (Dauerman and Tajima 1968; Suh et al. 1974; Fifer and Lannon 1975; Farber and Srivastava 1978). Discussed at some length by Warren et al. (2021), most variations of this theory posit that NO_2 formed by breaking nitrate-ester RO–NO_2 bonds complex with the catalyst and thereby drive the reversible process forward. Supporting this theory, it has been observed that temperatures near the burning surface of a catalyzed DBP are higher than those of its uncatalyzed counterpart, particularly at low pressures (Kubota et al. 1975). However, Warren et al. state that this theory appears to be limited to providing an explanation for super-rates; they did not believe it was capable of concomitantly explaining the plateau region. The results produced by my model suggest that it can. Indeed, as shown in Figure 10, it predicts that it will produce higher T^0 values, and as found by Kubota et al., the percentage change in those values will be higher at lower pressures.

5. Summary and Conclusion

As a step toward establishing a physics-based modeling framework with the potential to produce reliable burning-rate predictions for catalyzed DBPs, a three-phase model for simulating the deflagration of $O_{3,s}$ was formulated and applied. Seeking insight into the changes a catalyst would have to produce in the system's LP to generate $r(P)$ plots with super-rate and plateau regions, the impacts of heuristic changes to the LP's thermochemical kinetics mechanism were calculated and assessed. Plots comprising both super-rate and plateau regions were produced by combining 1) a reversible, one-step reaction with a relatively low barrier to the formation of O_l and $O_{2,l}$, and 2) lowering the (combined) enthalpies of O_l and $O_{2,l}$ relative to $O_{3,l}$'s from my best guess. It was also found that the super-rate produced by this scenario could be further increased by decreasing $P_{sat}^0(T)$ values in proportion to the concentration of the decomposition products at the liquid–gas interface.

Imagining mechanisms that might feasibly produce the heuristic changes in the system that were necessary to produce $r(P)$ plots with both super-rate and plateau regions, I posited a complexation reaction that subsequently proved to correspond to the complexation/chelation theory of super-rate burning. Significantly, the model produced results that put to rest a perceived shortcoming of this theory—namely, that it could not also explain/produce plateau burning. As such, it appears that with further development the framework could serve as a tool for screening the potential of alternatives to Pb-based catalysts for DBPs.

6. References

Anderson WR, Meagher NE, Vanderhoff JA. Dark zones of solid propellant flames: Critically assessed datasets, quantitative model comparison, and detailed chemical analysis. Combust Flame. 2011;158:1228–1244.

Brabets RI, McDonough JM. Density of liquid ozone. Journal of Chemical Physics. 1957;27:880–882.

Brabets RI, Waterman TE. Specific heat of liquid ozone. Journal of Chemical Physics. 1958;28:1212–1214.

Camp AT, Csanady ER, Mosher PR. Plateau propellant compositions. United States patent US4239561. 1980.

Chen CC, Anderson WR, McQuaid MJ. Computationally based predictions for the burning rates and flame structures of nitroglycerin doped with various small molecules. Army Research Laboratory (US); 2019. Report No.: ARL-TR-8721.

Dauerman L, Tajima Y. Solid-phase reactions of a double-base propellant. AIAA Journal. 1968;6:678–683.

Farber M, Srivastava RD. As mass-spectrometric investigation of the chemistry of plateau burning propellants. Combust Flame. 1978;31,309–323.

Fifer RA, Lannon JA. The effect of pressure and some lead salts on the chemistry of solid propellant combustion. Combust Flame. 1975;24:369–380.

Kee RJ, Rupley FM, Miller JA. CHEMKIN-II: a Fortran chemical kinetics package for the analysis of gas-phase chemical kinetics. Sandia National Laboratories (US); 1989. Report No.: SAND89-8009. https://doi.org/10.2172/5681118

Kee RJ et al. CHEMKIN collection, release 3.6: PREMIX. Reaction Design, Inc; 2000.

Kubota N, Ohlemiller TJ, Caveny LH, Summerfield M. Site and mode of action of platonizers in double base propellants. AIAA Journal. 1974;12:1709–1714.

Kubota N, Ohlemiller TJ, Caveny LH, Summerfield M. The mechanism of super-rate burning of catalyzed double base propellants. Symposium (International) on Combustion. 1975;15:529–537.

McQuaid MJ, Chen CC. Modeling the deflagration of ammonium perchlorate at pressures from 300 to 30000 psia. Part II: considerations besides the gas-phase, finite-rate chemical kinetics mechanism. Proceedings of the 45th JANNAF Combustion Subcommittee Meeting, 2014.

McQuaid MJ, Chen CC. A computationally based study of fizz zone effects on the linear burning rate of methyl nitrate. Proceedings of the 47th JANNAF Combustion Subcommittee Meeting, 2016a.

McQuaid MJ, Chen CC. A computationally based study of the chemical suppression of AP-HTPB composite propellant burning rates. Proceedings of the 47th JANNAF Combustion Subcommittee Meeting, 2016b.

McQuaid MJ, Chen CC, Veals JD. Simulating accelerating rate calorimetry experiments with a model having a detailed, gas-phase, finite-rate chemical kinetics mechanism: results for RDX. Proceedings of the 40th JANNAF Propellant and Explosives Development and Characterization Subcommittee (PEDCS) Meeting, 2017.

McQuaid MJ, Chen CC, Veals JD, Yeh IC. Detailed finite-rate chemical kinetics-based modeling of the decomposition of nitroglycerin in systems comprising liquid and gas phases. Proceedings of the 43rd JANNAF Propellant and Explosives Development and Characterization Subcommittee (PEDCS) Meeting, 2021.

McQuaid MJ, Stone CP. CYCLOPS3 burning rate predictor: PREMIX3_WPSB Version. DEVCOM Army Research Laboratory (US); 2024. Report No.: ARL-TR-9971.

Miller MS. Development of a 3-phase, detailed-kinetics, steady-state combustion model with heterogeneous reaction: application to frozen ozone. Proceedings of the 32nd JANNAF Combustion Subcommittee Meeting, 1995.

Miller MS. Three-phase combustion modeling: frozen ozone, a prototype system. Army Research Laboratory (US); 1997. Report No.: ARL-TR-1320.

Miller MS, Anderson WR. Burning-rate predictor for multi-ingredient propellants: nitrate-ester propellants. Journal of Propulsion and Power. 2004;20:440–453.

Miller MS, Anderson WR. Energetic-material combustion modeling with elementary gas-phase reactions: a practical approach. In: Yang V, Brill TB, Ren WZ, editors. Solid Propellant Combustion Chemistry, Combustion and Motor Interior Ballistics, Progress in Astronautics and Aeronautics, AIAA. 2000;85:501–531.

Sinha S, Patwardhan W. Burning of platonized propellants. Explosivstoffe. 1968;10:223–225.

Streng AG. Table of ozone properties. Journal of Chemical and Engineering Data. 1961;6:431–436.

Streng AG, Grosse AV. The density of solid ozone. Journal of the American Chemical Society. 1959;81:805–806.

Stull DR. Vapor pressure of pure substances. organic and inorganic compounds. Ind Eng Chem. 1947;39:517–540.

Suh NP, Adams GF, Lenchitz C. Observations on the role of lead modifiers in super-rate burning of nitrocellulose propellants. Combust Flame. 1974;22:289–293.

Veals JD, Chen CC, McQuaid MJ. Recent advances in modeling RDX combustion kinetics. Proceedings of the 46th JANNAF Combustion Subcommittee Meeting, 2019.

Warren LR, Wang Z, Pulham CR, Morrison CA. A review of the catalytic effects of lead-based ballistic modifiers on the combustion chemistry of double-base propellants. Propellants, Explosives, Pyrotechnics. 2021;46:13–25.

Waterman TE, Kirsh DP, Brabets RI. Thermal conductivity of liquid ozone. Journal of Chemical Physics. 1958;29:905–908.

Appendix. Formulae Employed to Compute Thermochemical and Transport Properties for Gas, Liquid, and Solid Ozone

This appendix provides the formulae that were employed to compute the enthalpies (H), heat capacities (c_p), and entropies (S) of the species in the three-phase model discussed in the main body of this report. In standard CHEMKIN format,[1] the formula were,

$$\frac{c_p(T)}{R} = a_1 + a_2T + a_3T^2 + a_4T^3 + a_5T^4 \qquad \text{(A-1)}$$

$$\frac{H(T)}{RT} = a_1 + \frac{a_2}{2}T + \frac{a_3}{3}T^2 + \frac{a_4}{4}T^3 + \frac{a_5}{5}T^4 + \frac{a_6}{T} \qquad \text{(A-2)}$$

$$\frac{S(T)}{RT} = a_1\ln(T) + a_2T + \frac{a_3}{2}T^2 + \frac{a_4}{3}T^3 + \frac{a_5}{4}T^4 + a_7 \qquad \text{(A-3)}$$

with (constant) coefficients $a_1 - a_7$ specified (as required) for atomic oxygen (O), molecular oxygen (O_2), and ozone (O_3) in each of the three phases—i.e., solid (s), liquid (l), and gas (g). R is the universal gas constant.

Table A-1 lists the coefficients specified to compute the thermochemical properties of gas-phase species. They were copied (verbatim) from Miller's paper[2] and used in all the simulations performed for the study.

Table A-1. Coefficients for computing thermodynamic properties for gas-phase species.[a]

	O_g		$O_{2,g}$		$O_{3,g}$	
	100–500K	**500–2500K**	**100–500K**	**500–2500K**	**100–500K**	**500–2500K**
a_1	2.88825887E+00	2.65382982E+00	3.45158664E+00	2.67007460E+00	4.52451445E+00	2.30793012E+00
a_2	4.70210727E-04	–3.14296633E-04	1.09681318E-03	3.02809039E-03	–1.07127953E-02	1.07264553E-02
a_3	–1.13844463E-05	2.57285985E-07	–8.43207843E-06	–2.15919761E-06	6.56158147E-05	–9.58603851E-06
a_4	3.08321341E-08	–9.59708843E-11	2.51928698E-08	7.51673207E-10	–1.10619800E-07	3.72488611E-09
a_5	–2.52095832E-11	1.35856771E-14	–2.08437806E-11	–9.75886533E-14	6.35707516E-11	–4.40613906E-13
a_6	2.91273618E+04	2.91828618E+04	–1.04325761E+03	–9.02757615E+02	1.57840489E+04	1.59590489E+04
a_7	3.05060374E+00	4.33860374E+00	4.86612215E+00	8.66612215E+00	4.08742597E+00	1.27774260E+01

[a] From Miller.[2] Specified for all cases.

Table A-2 provides the coefficients employed to compute the thermochemical properties of liquid-phase species. The coefficient values for $O_{3,l}$ were copied from Miller's paper[2] and specified in all the simulations performed for the study. The coefficients for O_l (Cases 1–3) and $O_{2,l}$ (all cases) were derived from fits to $H_{k,l}(T)$ values computed per

[1] Kee RJ, Rupley FM, Miller JA. CHEMKIN-II: a Fortran chemical kinetics package for the analysis of gas-phase chemical kinetics. Sandia National Laboratories (US); 1989. Report No.: SAND89-8009. https://doi.org/10.2172/5681118

[2] Miller MS. Development of a 3-phase, detailed-kinetics, steady-state combustion model with heterogeneous reaction: application to frozen ozone. Proceedings of the 32nd JANNAF Combustion Subcommittee Meeting, 1995.

$$H_{k,l}(T) = H_{k,g}(T) - \left(H_{O_3,g}(T) - H_{O_3,l}(T)\right). \quad \text{(A-4)}$$

The coefficients for O_l for Cases 4 and 5 were derived on the basis of a heuristic approach that is discussed in the main body of the report.

Table A-2. Coefficients for computing thermodynamic properties for liquid-phase species.

	O_l		$O_{2,l}$	$O_{3,l}$
	Cases 1–3	**Cases 4 and 5**	**All cases**	**All cases[a]**
a_1	6.24748390E+00	–1.00000000E+00	6.78542673E+00	7.22949170E+00
a_2	3.21054750E-02	0.00000000E-00	3.32125604E-02	3.38198289E-02
a_3	0.00000000E+00	0.00000000E+00	0.00000000E+00	0.00000000E+00
a_4	0.00000000E+00	0.00000000E+00	0.00000000E+00	0.00000000E+00
a_5	0.00000000E+00	0.00000000E+00	0.00000000E+00	0.00000000E+00
a_6	2.63375604E+04	1.58500000E+04	–3.83237721E+03	1.30170558E+04
a_7	1.52530187E+00	1.52530187E+00	2.43306108E+00	2.04371299E+00

[a] From Miller[2]

Table A-3 provides the coefficients employed to compute $O_{3,s}$'s thermochemical properties. They were copied from Miller's paper[2] and specified in all the simulations performed for the study.

Table A-3. Coefficients for computing $O_{3,s}$'s thermodynamic properties.[a]

	$O_{3,s}$
a_1	–4.55113905E+00
a_2	3.94994350E-01
a_3	–2.54310559E-03
a_4	–1.52073350E-05
a_5	1.70101860E-07
a_6	1.30576560E+04
a_7	Not specified

[a] From Miller.[2] Specified for all cases.

Table A-4 provides the coefficients employed to compute the transport properties of the gas-phase species. Miller[2] mentions that "multicomponent transport properties were evaluated and used in the gas phase" of his model. However, he published no other details about this aspect of his framework. The coefficients in Table A-4 were obtained from a CHEMKIN (Collection 3.7) manual.[3] I believe, but could not verify, that these coefficients date to before the distribution of CHEMKIN-II,[1] and that Miller likely would have used them.

[3] The CHEMKIN collection 3.7: transport core utility manual. Reaction Design; 2002.

Table A-4. Coefficients for computing the transport properties of gas-phase species.[a]

	Geometry	ε/k_B	σ	μ	α	Z_{rot}
O_g	0	80.0	2.750	0	0.0	0.0
$O_{2,g}$	1	107.4	3.458	0	1.6	3.8
$O_{3,g}$	2	180.0	4.100	0	0.0	2.0

[a] From The CHEMKIN Collection 3.7: Transport Core Utility Manual.[3] Specified for all cases.

List of Symbols, Abbreviations, and Acronyms

1D	one-dimensional
ARL	Army Research Laboratory
DBP	double-base propellant
DEVCOM	U.S. Army Combat Capabilities Development Command
FBRI	fractional burning-rate increase
GP	gas phase
HLK	Hertz–Langmuir–Knudsen
LP	liquid phase
NC	nitrocellulose
NG	nitroglycerine
Pb	lead
RDX	1,3,5-trinitro-1,3,5-triazinane
wt%	weight-percent

1 (PDF)	DEFENSE TECHNICAL INFORMATION CTR DTIC OCA
1 (PDF)	DEVCOM ARL FCDD RLB CI TECH LIB